Design and Development of a Low Cost Multi-Sensor Inertial Data Acquisition System for Sailing

Article *in* IEEE Transactions on Instrumentation and Measurement · January 2013

DOI: 10.1109/TIM.2013.2279004

2 authors, including:

Natalie Baddour
University of Ottawa
183 PUBLICATIONS **1,449** CITATIONS

SEE PROFILE

Design and Development of a Low-Cost Multisensor Inertial Data Acquisition System for Sailing

Alexandre Bergeron and Natalie Baddour

***Abstract*— This paper presents the development of an inertial measurement data acquisition system intended for use in sailboats. The variables of interest are three-axis acceleration, three-axis rotation, Global Positioning System (GPS) position/velocity, magnetic compass bearing, and wind speed/direction. The design focus is on low-cost microelectromechanical systems-based technology and demonstrating the validity of these technologies in a scientific application. A prototype is constructed and submitted to a series of tests to demonstrate functionality and soundness of the design. Contributions of this paper include the novel application of inertial measurement unit technology to a sailboat racing application, the integration of all instrumentation, creative ruggedized packaging, and emphasizing the use of low-cost commercial off-the-shelf technology.**

***Index Terms*— Accelerometer, data acquisition, GPS, gyroscope, inertial measurement units (IMUs), low cost, microelectromechanical systems (MEMS), sailing.**

I. Introduction

QUANTIFYING the motion of a vehicle is employed in numerous fields as a means to improve the underlying design, to control or use of the vehicle or parts thereof. For example, inertial measurement units (IMUs) have been applied to the analysis of vehicle dynamics [1]–[3], two-wheeled vehicles [4], [5], navigation for helicopters [6]–[8], tire deformation [9], navigation for land vehicles [10], [11], personal dead reckoning systems [12], [13], as well as navigation for submarines [14], and tractors [15]. With quantified knowledge of the motion, it should be possible to derive information on optimal approaches to vehicle handling, control, and navigation as well as potentially estimating applied loads and conditions. This paper aims to apply the same technique to the domain of sailing yachts; i.e., to quantifiably measure the motion of a sailboat while underway. Particular attention is given to the requirements of sailing, namely the marine environment and the recording of contextual wind information since wind is the driving force for a sailboat.

Work has been performed by other researchers on developing instruments for measuring wind for offshore marine energy applications [16], [17], and measuring wind for meteorological applications from a ship [18]. A sensor network was developed and tested to monitor air pressure on the top of a mainsail for sailboats [19]. On the other hand, real-time performance of a sailboat was estimated in [20], but only wind-speed, wind-angle, and boat speed were considered. The numerical prediction of the performance of a sailboat has been presented in [21] and [22], but contributions of those papers are simulations, not recording of actual data. A dynamometer was used to measure the forces on a sailboat in [23], but the only relevant information recorded on the motion of the boat was the speed, heel angle, along with wind speed and angle—no inertial measurements were made.

The fusion of IMUs with other types of data to study particular phenomena has been demonstrated in other fields. For example, IMUs have been combined with other sensors for navigation [24], accurate geolocation [25], orientation tracking [26], have been combined with RFIDs for indoor navigation [27] or combined with vehicle sensors to study the behavior of a vehicle driver [28]. Combined with GPS, a natural application of IMUs is for ship navigation [29]. Fusing of vision with inertial sensing has received a great deal of attention from the mobile robotics community [30], [31].

Electronic devices which measure and record motion have found numerous applications in many types of vehicles, as mentioned above. However, there is no documented evidence in the literature of an instrumentation system that records dynamical sailboat motion data in conjunction with real-time contextual wind data. The simultaneous real-time recording of the wind data is important as it is the context for the motion that is being recorded. Thus, the primary contribution of this paper is the design and development of a marine data acquisition device, which successfully acquires relevant data on the motion of a sailboat during a race, including contextual real-time wind data. The device is designed with the intent to form the basis of a platform for further experimentation on the motion of a sailboat.

II. System Architecture

A. Design Requirements

The design requirements for the proposed marine data acquisition system can be outlined as follows: 1) correctly record the motion of a sailing yacht while underway; 2) determine and record the spatial position of the sailing

Manuscript received March 13, 2013; revised June 19, 2013; accepted June 20, 2013. Date of publication September 4, 2013; date of current version January 2, 2014. The Associate Editor coordinating the review process was Dr. Subhas Mukhopadhyay.

The authors are with the Department of Mechanical Engineering, University of Ottawa, Ottawa, ON K1N 6N5, Canada (e-mail: aberg098@uottawa.ca; nbaddour@uottawa.ca).

Color versions of one or more of the figures in this paper are available online at http://ieeexplore.ieee.org.

Digital Object Identifier 10.1109/TIM.2013.2279004

TABLE I
DESIGN SPECIFICATIONS

Measured Quantity	Sensor	Range	Sensitivity
Linear Acceleration	Accelerometer	+/- 30 m/s^2	0.1 m/s^2
Rotational Velocity	Gyroscope	+/- 200 º/s	5 º/s
Magnetic Heading	Compass	0-360º	1º
Relative Wind Speed	Anemometer	0-50 knots	1 knot
Relative Wind Heading	Weather vane	Cardinal references (N, NE, E, etc.)	π/8 radians
GPS Heading	GPS	0-360º	1º
GPS Speed	GPS	0-50 knots	0.1 knot
GPS Position	GPS	N/A	+/- 50m
GPS Time	GPS	N/A	1 second
Measurement Interval	Timer	0-50000 µs	1 µs

yacht at any time in customary units of latitude and longitude; 3) provide contextual information regarding wind conditions; 4) withstand the rigors of the environment found on any boat, such as the possibility of water or the impact of waves; and 5) minimize the cost of parts of the prototype. The variables of interest along with the relevant sensors, required measurement range and sensitivity are shown in Table I.

The accelerometer specifications are based on what is typically used for measurement in automobiles. Airbag control accelerometers are typically triggered at 50 g (490 m/s^2) [32], [33], while the max acceleration seen under braking or cornering by a racing car is typically around 1.5–2 g (14.7–19.6 m/s^2) [34], [35]. As a sailboat typically moves much more slowly than a car, this limit will be used as a guideline.

The specified gyroscope range is based on a worst case scenario: capsize of a boat. Prior experience shows that this rare occurrence tends to happen rather quickly. It is estimated that a capsize involves the rotation of the boat by approximately 90° in a very short interval of 0.5 s. This equates to 180°/s.

The GPS specifications are based on what is normal for commercial GPS modules subjected to civilian restrictions [36].

The sailing community's convention is to measure wind speed in knots. Typically, sailing is possible from between 5 and ∼40 knots [37] and only in extreme case are boats sailed in storm-force winds. Since wind speed measurements will be relative to the moving craft, allowance is made to account for the possibility that the relative wind speed could be null or higher than the true wind speed.

Wind direction is conventionally given as a cardinal point, such as north (0°) or north-east (45°). These represent rough headings in increments of 45°. In maritime conventions, a further measure of precision is given by dividing the headings, e.g., north–north–east (22.5°). Since the measurement of wind direction on a sailboat is affected by a multitude of factors, not the least of which is due to the motion of the craft itself, it is assumed that there is no need to have any greater resolution than 22.5° for relative wind direction measurement in order to provide sufficient contextual information.

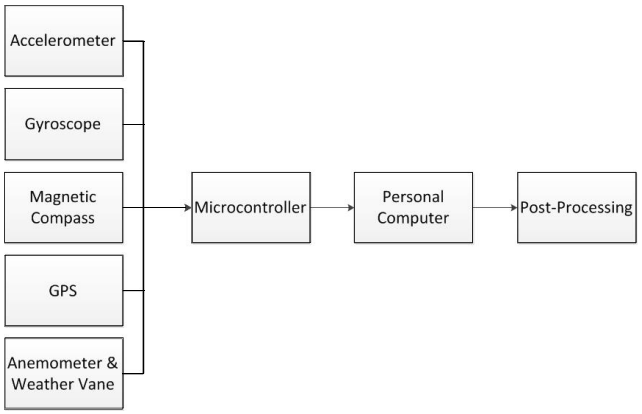

Fig. 1. Proposed system.

Battery life requirements are set to exceed the duration of the average club race, which may last for 2–3 h. With this in mind, the minimum battery life for the device should be 6 h. 6 h was demonstrated to be more than sufficient to achieve the goals of the instrument. Even if used for a regatta, the boats are rarely out of the water for more than 5–6 h at a time. For smaller boats, the system must be standalone and compact in order to be as unobtrusive and versatile as possible. Boats partaking in long-distance, multiday races would typically be larger and thus would have onboard power that would permit a battery to be recharged while sailing.

B. System Architecture

It should be noted that some of the system requirements may be fulfilled by any modern smartphone that contains embedded magnetic sensors, accelerometers, GPS, and gyroscopes. However, the difficulty with this is that there are currently no wind instruments available that could be interfaced with a smartphone. Currently available wireless wind instruments are expensive, but more importantly operate on a proprietary standard (do not use any standard protocols such as Bluetooth) and only communicate with another proprietary system that offers no logging capability or interface with compass, inertial, or GPS sensors. The instrumentation difficulty lies in the capability of currently available wind instruments, not in the smartphone itself.

The recording of wind data is instrumental to a sailing performance-related instrument as the wind data is the context for the motion that is being recorded. Without context, there is no hope of understanding the dynamics of the boat or its crew. Thus, to achieve the design requirements, the architecture of the proposed system is shown in Fig. 1. The chosen sensors are the Razor 6DOF IMU for acceleration and rotational rate measurements, the HMC6352 Digital Compass for magnetic heading, the Venus 634LPx GPS receiver, and an anemometer and wind vane to measure the wind information. Two options are provided to link the AxonII microcontroller with a personal computer; these modes are USB output and secure digital (SD) cards.

III. Hardware

A. Microcontroller

This proof of concept system is built around the Society of Robot's AxonII [1] microcontroller package. The AxonII is based on Atmel's ATMega640 8-bit processor, which incorporates 64 KB of programmable memory and includes 16 channels of 10-bit A/D conversion. This processor supports three universal asynchronous receiver transmitter (UART) ports for interfacing with sensors and dedicates an additional UART for USB communication with a PC. There is also support for one interintegrated circuit (I^2C) port.

The integrated development environment for the AxonII is Atmel's AVR Studio, which is a complimentary product for their line of microprocessors: the programming language is C-based. The AVR studio library specific to the AxonII is the open-source WebbotLib [38], is intended for robotics applications. WebbotLib contains the necessary header files to interface with all required sensors. The AxonII microcontroller package retails for US$118.00.

B. Accelerometer and Gyroscopes

Full 3-axis linear and rotational accelerations are measured on a combination IMU board sold by Sparkfun Electronics under the name Razor 6DOF IMU. This device is based on existing inexpensive microelectromechanical systems (MEMS). They are compact and draw very little power. This type of combination IMU board is increasingly being chosen for navigation and positional instruments [24], [39].

A 3-axis accelerometer, in the form of the analog devices ADXL335, provides the required linear measurements. It has a range ± 3g and is intended for use in cost-sensitive motion sensing applications. Two gyroscopes provide angular measurements, both manufactured by STMicroelectronics. There are currently no inexpensive 3-axis MEMS devices available, hence the need for at least two separate devices. Both these gyroscopes have a $\pm 300°$/s measuring range.

All gyroscope and accelerometer outputs are voltages, implying that they are interfaced with the AxonII using 6 A/D converter ports. WebbotLib handles the conversion from voltage to the proper engineering units, whether m/s or degrees/s. This particular combination IMU board retails for US$59.95.

C. GPS

In order to satisfy packaging requirements, the GPS needed to have a remote antenna due to the possibility of mounting the data acquisition package where signal reception could be troublesome. Due to this, a GPS device with separate antenna was specified. It is based on the MicroModular Technologies MN5010HS GPS receiver chip, which is a SiRF III chipset and is sold as the GPS MicroMini with SMA connector by Sparkfun Electronics. This GPS sensor was chosen due to its low cost and ability to satisfy the specified design requirements. The SMA connector packaged with this sensor is coupled with an external antenna, in this case one with a magnetic mount and 5 m cable. The antenna has a gain of 26 dB and a voltage standing wave ratio of <2.0. Interfacing the GPS with the AxonII is done through one of the UART ports on the AxonII. The necessary drivers to interpret standardized string outputs from the GPS are included in the WebbotLib library. As with most common GPS devices, the output strings follow the National Marine Electronics Association standard 0183 (NMEA 0183) [37]. This GPS device retails for US$79.95 and the external antenna retails for US$12.95. Since sailboats operate in a open environment, the GPS should provide the requisite location, heading, and speed measurements [25]. High accuracy (centimeter-level) geolocation is not required for this application.

D. Magnetic Compass

Measuring the compass heading is handled by a Honeywell HMC 6352 solid-state magneto-resistive-based device. The integrated circuit does all of the necessary interpretation and converts the output to a magnetic heading in degrees directly. Sensor resolution is 0.5° with 1° of repeatability. The outgoing signal is relayed to the AxonII through the I^2C connection port. Similarly to the traditional magnetic needle compass, this solid-state device is subject to the same limitations, such as interference from large metal structures or close proximity magnetic fields [40]. This magnetic compass device retails for US$34.95.

E. Computer Interface

The AxonII uses an integrated Silicon Labs CP210x USB to UART bridge chip to convert its lower level UART signals to a more convenient USB format. The AxonII's output signals are then interpreted by a Windows PC through a virtual COM port, which is treated like an older style 9-pin (RS-232) serial port. The output signals are further interpreted, compiled, and recorded using MATLAB R2010a technical computing software.

In order to maximize the portability of the inertial measurement data acquisition system prototype, it can be configured to eliminate the need for a PC to record the data during the actual testing. This is desirable, especially on rough seas where water ingress or shock can create problems with a traditional computer or laptop. Initial testing of the prototype used a computer, but it quickly became apparent that this was not suitable. Hence, a standalone mode was developed as explained above. This completely eliminated the need for a PC during data acquisition and also eliminated need to protect the computer since the PC is no longer required.

This standalone configuration removes the need for a PC by using multimedia cards (MMC) or SD cards as the destination to which the AxonII sends measurement data to be recorded. Data are written to the digital storage cards in the form of .txt files, which store each sequence of measurements as a line of comma-separated variables representing a specific measurement. Once one line representing a sequence of measurements is complete, the next sequence is stored on the next line of the .txt file. Further interpretation is needed to convert the accelerometer, gyroscope, wind heading, and wind speed into useable measurements. This is carried out during post-processing on a computer.

Once the PC was eliminated, the device became quite robust—recording was started before heading out on the water and stopped when the boat returned to dock. With the PC eliminated, the device was successfully used without any shock or water issues.

F. Wind Instruments

Although improvements to the design of wind sensors have been made to address specific applications [41]–[43], simple and robust instruments were chosen for this prototype. Both anemometer and wind vane are from a kit imported by Argent Data Systems as the "Weather Sensor Assembly p/n 80 422" [44]. The anemometer in the Weather Sensor Assembly is a rotating three cup device; the force of moving air causes the rotation of the cups about a vertical axis. Inside the anemometer, a reed switch is activated twice every rotation by completing an electrical circuit. This generates a series of pulses, the frequency variations of which can be related to speed over a short interval of time (in this case one second). The actual counting and conversion is performed during post-processing. The weather vane is a flat vane type, free to rotate about a vertical axis to maintain alignment with the wind's direction. Internally, the wind vane uses a voltage-divider type of sensor and measures wind direction in increments of 1/16th of a full circle (22.5° increments). The voltage outputted by the weather vane is a function of the varying resistance of the sensor [45]. The ADC channel value is recorded and interpretation of the raw data is performed later during post-processing.

G. Physical Setup and Wiring

In order to contain all of the necessary electronics, sensors, batteries, and power circuits, a container is needed. A major concern for the application is waterproofing and resistance to corrosion. With the exception of the waterproof GPS antenna, everything is packaged in a Pelican 1120 Case.

All of the hardware components are interfaced to the AxonII following the wiring schematic shown in Fig. 2. The HMC6352 compass, the Razor 6DOF IMU, and the Venus 634LPx are all soldered on a 0.100" pitch prototyping board using standardized pin headers, which also provides structural mounting for the components. Wiring headers are soldered onto the prototyping board; this allows for the connection of wires between the AxonII and the sensor components. The connectors used are standard Molex 0.100" pitch connectors.

Other components including the power switch, battery, and secure digital storage media interface are connected to the AxonII using similar connectors, but are not physically soldered to the prototyping board for ease of access.

One limitation of the AxonII microcontroller is the small number of available 3.3 V outputs, in fact there is only 73 mA of current available. To overcome this limitation, it was necessary to put into place a separate 5–3.3 V conversion integrated circuit using an NTE1904 Positive 3 Terminal Voltage Regulator. This is powered by one of the AxonII's 5 V outputs and is able to accommodate power for the compass,

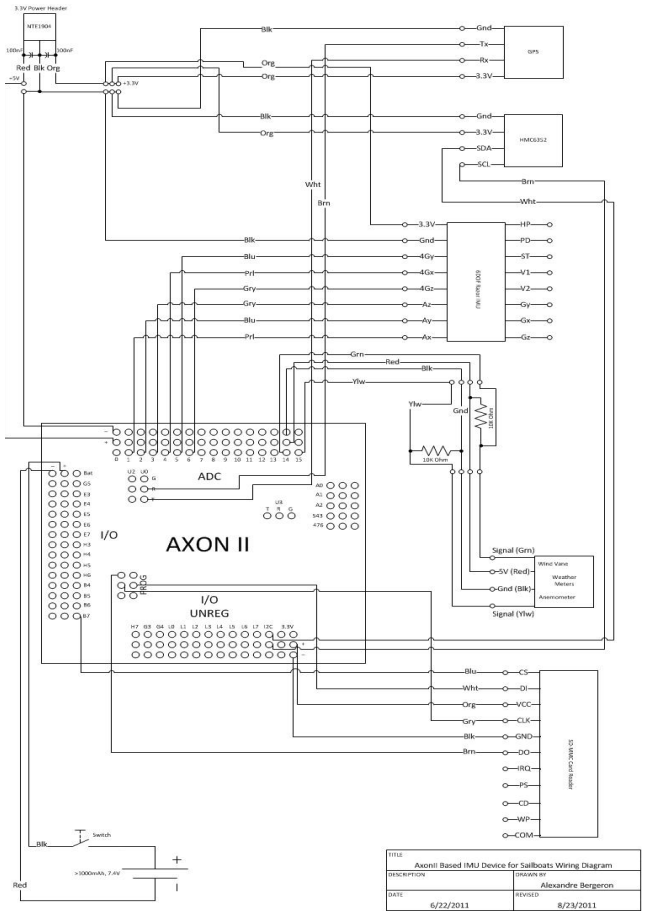

Fig. 2. Data acquisition prototype wiring diagram.

GPS, and Razor IMU. The onboard 3.3 V ports are used only to power the MMC/SD card interface.

The GPS is designed to send standard NMEA message strings at a preset Baud rate through a generic UART port. Since the Venus 634 LPx can function at several Baud rates, it is important to configure the AxonII UART port Baud rate to match the GPS output Baud rate. First, it is necessary to perform a one-time configuration of the Venus GPS to match its output Baud rate to the AxonII's default 115 200. At the same time, the GPS refresh rate is set to its maximum possible value of 10 Hz.

The GPS NMEA string messages are sent to the AxonII according to the standard format described in NMEA standard 0183 [37]. Webbotlib provides functions that interpret NMEA strings from a generic GPS device. This standard library function was further modified to optimize performance. The Honey well HMC6352 digital compass is set up to use an I^2C interface as a slave component. Internally, it is accessed at the address 0X42 and comes from the factory set up to simply output its reading continuously. It is interfaced using functions from Webbotlib. This prebuilt library simplifies the programming required on the AxonII in order to interface the sensor correctly. However, some further set-up is required to send a message to the compass in order to modify its default refresh rate from 1 to 20 Hz. This implies a one-time configuration of the compass by sending it the correct message.

Interfacing of the accelerometers in the Razor 6DOF IMU is achieved through an ADC sampling of the output voltages. This requires proper configuration and identification of the AxonII's built-in ADC channels: i.e., channel 1 is x-axis acceleration, channel 2 is y-axis acceleration, etc. This channel numbering is shown on the wiring diagram in Fig. 2.

The SD card used for the standalone interface mode requires the AxonII microcontroller to treat it as a disc. This is done through an SPI bus interface set up using Webbotlib functions, which allow the setup of an SPI bus using a standard UART port. Data is stored in a buffer until sufficient data is accumulated in the buffer to fill one block on the SD card. This buffer is also set up using standard Webbotlib functions.

IV. Measured Signals

A. Variables of Interest

Inertial data is measured in three orthogonal axes, x,y, and z, as is conventional in a Cartesian coordinate system. This inertial data consists of linear and rotational acceleration along x, y, and z axes. This is supplemented by GPS position data as well as GPS heading and speed information. Finally, relative wind speed and heading, as well as magnetic heading are also measured. These measurements are repeated in sequence by the AxonII microcontroller; once one line is complete, the next line begins.

V. Validation and Testing

Validation of the instrument was performed via tests conducted in the laboratory, and also in a car, bicycle, and boat. These tests are described herein.

A. Laboratory Testing

Initial tests were simple bench tests carried out in the laboratory to verify the correct working of all the sensors. The measured battery life for the prototype was at least 9 h. In order to accurately verify the wind speed, the anemometer was mounted against a constant wind source in the form of a desktop oscillating fan and compared against the measurements made by an independent, portable anemometer (SpeedTech WindMate WM-200, with a claimed accuracy of $\pm 3\%$). The prototype anemometer was found to be consistently within 5.5% of the WM-200 wind speeds and generally underestimated the wind speed as compared to the WM-200. Validating the wind direction was accomplished by rotating the weather vane through all possible headings. This was done by rapidly spinning the weather vane and allowing it to rotate freely, artificially producing motion. The measured wind heading showed an increasing heading over time, peaking at 337.5° before returning to zero. This process is periodical because of the spinning motion of the weather vane.

While in PC (USB) interface mode, the prototype data acquisition system was left to record data over a period of 1 h with the purpose of examining the length of the measurement interval. The average measurement interval for this case was found to be 0.01031 s with a standard deviation of 0.000215 s, implying a measurement frequency of 97.08 Hz for the PC interface mode. In standalone (SD card) interface mode, the same test was repeated and found to yield an average measurement interval of 0.01028 s with a standard deviation of 0.00354 s. This equates to a measurement frequency of 97.22 Hz.

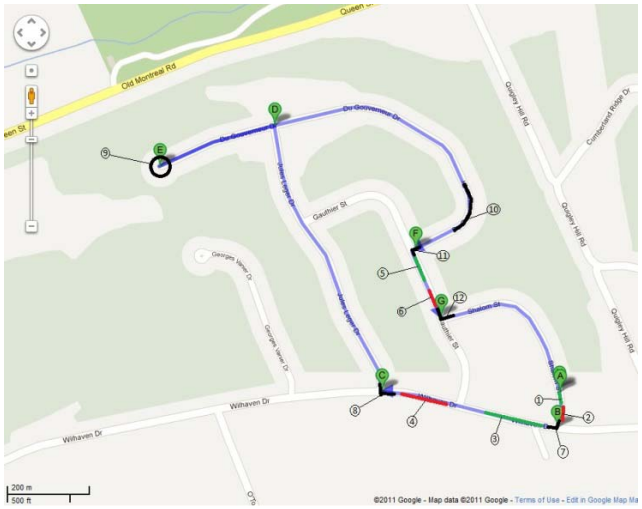

Fig. 3. Test circuit and event locations.

B. In-Car Testing

The first phase of dynamic testing was done in a moving car. This test used an easily repeatable 5-min test circuit on low-speed roads, shown in Fig. 3. Several trials of the test were conducted with different drivers completing several laps of the same circuit.

The chosen track consisted of a circuit, which was divided into sections A through G and 12 distinct events for the purpose of analysis. These 12 events are: 1) accelerate after A; 2) decelerate before turn B; 3) accelerate after turn B; 4) decelerate before turn C; 5) accelerate after turn F; 6) decelerate before turn G; 7) right-hand turn at B; 8) right-hand turn at C; 9) full counter-clockwise circle at E; 10) sweeping left-hand turn before F; 11) left-hand turn at F; and 12) left-hand turn at G. The radius of the turn at event 10 was estimated to be about 65 m via Google earth.

The recorded GPS position plot was overlaid on the test circuit map and found to correlate with the map. GPS speed also correlated well with observed speeds during the test runs.

Due to the relatively flat nature of the test course and the fact that the automobile exhibited little roll during the test session, the only meaningful acceleration data to be used for further analysis were on the fore-aft and lateral axes, x and y, respectively. In order to try to better quantify the accuracy of the measurements and to compare them to an expected value, a basic analysis was carried out by examining specific events. For x-axis accelerations, events 1 through 6 are relevant whereas for y-axis accelerations, event 10 was used.

1) X-Axis Acceleration Analysis: The verification of linear straight-line accelerations as measured by the accelerometer is based on the GPS measurements. Starting and ending

positions for each of the events chosen for analysis were via the latitude and longitude, and then correlated with a corresponding start and end times. Once the start and end times were known, an average of the accelerometer-measured accelerations between the start and end times was computed. This was then compared to acceleration calculated from the change in measured GPS speed between the start and end times by assuming a constant linear acceleration. For all of the events in each test, a percentage difference was calculated between the actual accelerometer-measured value and the approximate value calculated via the GPS measurement. On average, there was found to be a 27% difference between the actual and calculated values, with a standard deviation of 19%.

The differences between the actual accelerations and the estimation provided by the linear acceleration based on GPS speed measurements can be explained by several factors. Primarily, the actual measured accelerations are not constant, therefore the use of a constant acceleration to estimate the acceleration from GPS speed will introduce errors. However, the assumption of a constant acceleration is sufficient to confirm that the measurements produced by the accelerometer are of the correct order of magnitude and close to the expected value. Additionally, the GPS speed measurements were refreshed at a much slower rate (10 Hz) than the accelerometer (∼97 Hz), also introducing minor errors.

2) Y-Axis Acceleration Analysis: Y-axis acceleration analysis focuses on event 10, a constant radius right hand turn. The accelerometer-measured y-axis accelerations were compared to an estimate based on the average speed carried by the vehicle through the turn. For a constant radius turn, the inward-pointing y-acceleration should satisfy $a_y = v^2/r$, where v is the speed of the vehicle and r is the radius of the turn. The average difference between the average-measured lateral acceleration and the calculated (expected) acceleration was found to be 17% with a 2% standard deviation.

Deviations between the estimate and the actual measurements can be explained by a few factors. First, the speed of the car during the turn is not constant for the duration of the turn, therefore NOR is the lateral acceleration. However, the formula for inward-pointing acceleration holds for any instant in time so could be applied at any point in time. Further, any minor misalignment of the x, y, z axes of the prototype box with respect to forward/lateral/vertical axes with respect to the ground implies that the x, y, z axis accelerations that are measured by the instrument are in directions other than what might be considered to be "true" forward, lateral, or vertical directions with respect to the ground. For example, it was assumed that the car does not roll, however, any minor rolling of the car will affect the measured y-axis accelerations. The average GPS speed value employed in the estimate is calculated over the duration of the event. In reality, it is not constant. Once the road speed limit has been reached, there are still some variations introduced by driver error and road conditions. These same errors carry over in the estimation. As previously mentioned, the GPS also has a much lower sampling rate than any of the accelerometers.

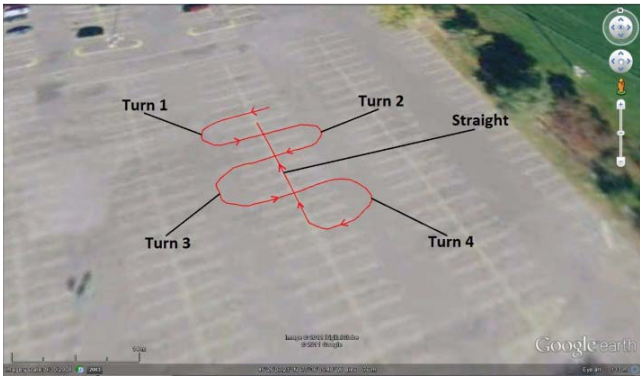

Fig. 4. Bicycle test circuit.

3) Gyroscope: In order to quantify the accuracy of the gyroscope, the obtained yaw measurements were compared to an expected value obtained via the GPS. Events 7 through 12 were analyzed. Event start and end times are chosen using the vehicle's position as the trigger. The calculated estimate was based on the GPS heading change over the chosen start and end points of a given maneuver: e.g., in event 7, the car changes heading by 81°. Using the time stamps, time required to complete the maneuvers was calculated. An average rotational (yaw) rate was then estimated by dividing the heading change with the total time needed to complete the maneuver. This particular estimate also assumes that the vehicle is yawing at a constant rate. Overall, the average difference between the estimated yaw rate values and the measured values was 28% with a standard deviation of 21%. The principle differences between the actual measured rotational rate and the estimate based on the GPS heading were be attributed to similar factors to those outlined previously: the non-constant nature of the yaw rate and the lower GPS refresh rate.

The constant radius right-hand turn at event 10 was also be analyzed from a different point of view. By using the gyroscope's rotational rate measurement and maintaining the assumption that the turn at event 10 had a constant radius of 65 m, the speed at which the car was travelling through the turn was calculated via $v = \omega \times r$, where ω is the yaw rate and r is the radius of the turn. The resultant speed was then compared with the actual GPS average speed for event 10. Overall, the average percent difference for this particular comparison was 24%, with a standard deviation of 2%. Any difference is explained by the same factors as the previous gyroscope approximations, lower GPS refresh rate, and the non-constant nature of the actual yaw rate.

C. Bicycle Testing

The prototype data acquisition system was mounted to the rear of a common road-going bicycle, atop a pannier style luggage rack. This provided a flat mounting surface, which was easy to align with the bicycle's direction of travel.

The test circuit itself was physically marked on the surface of a paved car park with chalk, making use of painted lines normally used to align parked vehicles. The chosen test circuit had pairs of identical constant radius turns in the left and right directions. The actual layout is shown in Fig. 4.

Each turn was 180° and arranged in matching left and right pairs: turns 1, 2 were small radius turns and turns 3, 4 have radii 50% larger than the first pair. The approximate total length of the test circuit, as measured by Google earth, is 113 m. Turn 1 was a left-hand turn with 2.75 m radius. Turn 2 was a right-hand turn with 2.75 m radius. Turn 3 was a left-hand turn with 4.13 m radius. Turn 4 was a right-hand turn with 4.13 m radius. Several test runs were carried out in two different ways: first using a rider who was tasked with following the prescribed track as closely as possible and second by pushing the bicycle around the circuit while on foot.

Riding the bicycle allows for higher speeds down the straight portion of the track and wider radius turns 3 and 4 when compared to pushing the bicycle. However, riding the bicycle implied difficulty in maintaining a smooth and precise heading especially on the tight portions of the course. Pushing the bicycle allowed the user to follow the track much more precisely and smoothly while generally maintaining a constant roll angle through turns. It was also possible to increase the roll of the bicycle through the corners when pushing it. Video recordings of each test run can be seen in the video. The camera was mounted to the chest of the cyclist.

1) Roll Angle Estimation: Due to the bicycle's inherent leaning into corners, the accelerometer's measurements were used to estimate the heeling (roll) angle. It was assumed that the bicycle does not pitch and that the roll angle is stable once the bicycle has transitioned from a vertical to rolled orientation. For all cases, the test circuit was traversed at least three times. The roll angle estimation was performed by assuming that the expected acceleration to be measured was due to gravity (which should be downward) and the centripetal acceleration (which should point into the center of the turn and have magnitude v^2/r). Using the heel angle estimation equation obtained via these assumptions, heel angles were numerically calculated using actual test data, averaged out over approximately 0.5 s. Although each turn lasted for at least 4 s, a half-second window proved adequate to estimate a roll angle.

The average estimated roll angle for turn 1 was 4.97°, with a standard deviation of 0.87°. This is well correlated with the video taken during the test. The average estimated roll angle for turn 2 was 5.90°, with a standard deviation of 3.9°. Turn 2 proved to be the most difficult for the rider to execute smoothly. Because the rider was able to carry more speed entering turn 2 as compared to turn 1, he compensated by rolling the bicycle to a greater extent compared to turn 1. The disadvantage of this was the rider's tendency to overcompensate by exaggerating the roll. This instability resulted in more oscillations in the bicycle's roll angle, which is problematic with the basic assumption of the estimation: that the roll angle remains steady after the rider has transitioned from his vertical orientation to a leaned orientation. This can be directly observed by video and is confirmed by the larger standard deviation in the roll-angle estimate for turn 2, as compared with turn 1.

The average estimated roll angle for turn 3 was 6.46° with a standard deviation of 3.5°, slightly more than the roll angle of turns 1 and 2. Because turn 3 had a larger radius than the two previous corners, it could be taken as a higher speed and increased roll angle.

The final estimation was intended for comparative purposes where the bicycle was intended to be upright and have no roll angle. The average estimated roll angle for riding in a straight line was measured at 1.2° with a standard deviation of 0.33°. Riding in straight lines is smoother as speed increases and there is an inherent rolling oscillation caused by the rider shifting his weight side-to-side while pedaling. As the video illustrates, the bicycle did indeed exhibit oscillation, which is why the roll angle estimation yields non-zero results.

For a different set of tests, the cyclist pushed the bicycle while walking on the right-hand side of the bicycle when facing forward. The average estimated roll angle for turn 1 was 14° with a standard deviation of 1.36°. The estimated roll angle for turn 3 was 12° with a standard deviation of 0.72°. Since the rider was pushing the bicycle and had good control of the roll angle, the roll angles for this case were much larger with smaller standard deviations as compared to the case where the bicycle was being ridden.

D. Boat Testing

The final phase of dynamic validation testing was to obtain data directly from a sailboat while underway. Physical installation of the prototype data acquisition unit proved challenging, bearing in mind that the entire installation needed to be temporary and require that no permanent changes be made to the test vessel. Additional installation considerations required that the unit be aligned properly with the sailboat's forward and lateral axes while being horizontal when the boat is unladen and stationary.

A J/24 was used as the testing boat—a popular 24-foot, racing keel boat. The most suitable location for aligning the unit proved to be the flat floor intended as the fore berthing area in the J/24. The flat floor provided good support and, in combination with the vertical bulkhead, aligned the unit properly. Rubberized plastic C-clamps were used to secure the unit into position without the need for permanent fasteners or other damaging methods. The wind instruments required external mounting. Ideally, these should be placed at the top of the mast, in order to get the best possible wind readings, unimpeded by the disturbances caused by sails or rigging. Due to the difficulty in actually accessing the top portion of the mast to install temporary instruments, these were positioned on the safety railing, which lines the periphery of the deck. Temporary mounting was accomplished using plastic cable ties. Cable management for the wind instruments was important due to the fact that they must traverse the cockpit area without impeding the crew's operation of the boat or being accidentally removed. It was not possible to route the cable through the hull so the wiring was attached to the side of the cockpit using residue-free painter's tape.

The final installation consideration was finding a suitable location for a portable computer. This needed to be shock proof and absolutely dry since only a standard netbook format computer with no waterproofing was used. A larger Pelican 1400 case containing the computer was used and this fit neatly in the J/24 galley's sink.

Operating the prototype data acquisition could be performed in one of two modes, PC interface (USB) mode or standalone (SD card) mode. In practice, the PC interface mode was much harder to implement correctly because of limitations imposed by the laptop. These limitations included battery life of the laptop and the inability of the laptop to withstand shock loads. On several occasions, the net book suffered crashes due to hard drive-related errors. This necessitated a system reboot and all gathered test data was lost. Once the laptop is stowed, the user may not notice the exact moment of failure, which resulted in lost testing time and data.

The standalone (SD card) mode proved to be free of these issues because it eliminated the need for an on-board personal computer. In fact, the standalone mode proved much easier to use, the user simply powered up the prototype and initiated the recording, knowing that the device had at least 9 h of battery life and recording time. Once the race was over, the recording was simply stopped and the unit powered down.

The two main environmental factors encountered by the data acquisition system were shock loading and water. The crashing of the boat through the waves did become uncomfortable and disorientating below deck. However, these repeated impacts over several hours did not adversely affect the electronics.

The installation of the prototype data acquisition system was very near to the mast, where water could enter when waves washed across the deck. These conveniently landed directly atop the Pelican case repeatedly and proved harmless to the device contained within.

VI. Conclusion

The total cost of this prototype device was US$305.80 prior to the applicable sales taxes. It demonstrated the ability to measure and record all the information in the design requirements at a useable data rate of up to 101 Hz. This data rate is comparable to many mid-range commercial and scientific IMU data logging packages with a much higher price point. This novel prototype featured the simultaneous acquisition and recording of compass, inertial and GPS data, along with real-time, on-board wind data. All details regarding the development and testing of the prototype, including all the specification sheets and the software code can be found in [46], available online.

References

[1] G. A. MacDonald, "A review of low cost accelerometers for vehicle dynamics," *Sens. Actuators A, Phys.*, vol. 21, nos. 1–3, pp. 303–307, Feb. 1990.

[2] J. Ryu and J. C. Gerdes, "Integrating inertial sensors with global positioning system (GPS) for vehicle dynamics control," *J. Dyn. Syst., Meas., Control*, vol. 126, no. 2, pp. 243–254, 2004.

[3] J. A. Pytka, P. Tarkowski, S. Fijałkowski, P. Budzyński, J. Dabrowski, W. Kupicz, and P. Pytka, "An instrumented vehicle for offroad dynamics testing," *J. Terramech.*, vol. 48, no. 5, pp. 384–395, Oct. 2011.

[4] I. Boniolo, S. M. Savaresi, and M. Tanelli, "Lean angle estimation in two-wheeled vehicles with a reduced sensor configuration," in *Proc. IEEE ISCAS*, May 2012, pp. 2573–2576.

[5] L. Gasbarro, A. Beghi, R. Frezza, F. Nori, and C. Spagnol, "Motorcycle trajectory reconstruction by integration of vision and MEMS accelerometers," in *Proc. 43rd IEEE CDC*, vol. 1. Dec. 2004, pp. 779–783.

[6] Z. Taha, Y. R. Tang, and K. C. Yap, "Development of an onboard system for flight data collection of a small-scale UAV helicopter," *Mechatronics*, vol. 21, no. 1, pp. 132–144, Feb. 2011.

[7] J. Wendel, O. Meister, C. Schlaile, and G. F. Trommer, "An integrated GPS/MEMS-IMU navigation system for an autonomous helicopter," *Aerosp. Sci. Technol.*, vol. 10, no. 6, pp. 527–533, Sep. 2006.

[8] M. W. Achtelik, S. Lynen, S. Weiss, L. Kneip, M. Chli, and R. Siegwart, "Visual-inertial SLAM for a small helicopter in large outdoor environments," in *Proc. IEEE/RSJ Int. Conf. IROS*, Oct. 2012, pp. 2651–2652.

[9] S. M. Savaresi, M. Tanelli, P. Langthaler, and L. Del Re, "New regressors for the direct identification of tire deformation in road vehicles via 'in-tire' accelerometers," *IEEE Trans. Control Syst. Technol.*, vol. 16, no. 4, pp. 769–780, Jul. 2008.

[10] S. Sukkarieh, E. M. Nebot, and H. F. Durrant-Whyte, "A high integrity IMU/GPS navigation loop for autonomous land vehicle applications," *IEEE Trans. Robot. Autom.*, vol. 15, no. 3, pp. 572–578, Jun. 1999.

[11] C.-Y. Liu, C.-A. Lin, K.-W. Chiang, S.-C. Huang, C.-C. Chang, and J.-M. Cai, "Performance evaluation of real-time MEMS INS/GPS integration with ZUPT/ZIHR/NHC for land navigation," in *Proc. 12th Int. Conf. ITST*, 2012, pp. 584–588.

[12] L. Ojeda and J. Borenstein, "Non-GPS navigation for security personnel and first responders," *J. Navigat.*, vol. 60, no. 3, pp. 391–407, 2007.

[13] O. Bebek, M. A. Suster, S. Rajgopal, M. J. Fu, X. Huang, M. C. Cavusoglu, D. J. Young, M. Mehregany, A. J. van den Bogert, and C. H. Mastrangelo, "Personal navigation via high-resolution gait-corrected inertial measurement units," *IEEE Trans. Instrum. Meas.*, vol. 59, no. 11, pp. 3018–3027, Nov. 2010.

[14] M. Bennamoun, B. Boashash, F. Faruqi, and M. Dunbar, "The development of an integrated GPS/INS/sonar navigation system for autonomous underwater vehicle navigation," in *Proc. Symp. Aut. Underwater Veh. Technol.*, 1996, pp. 256–261.

[15] Y. Shen, Z. Zhu, and E. Mao, "Double-fuzzy Kalman filter based on GPS/IMU/MV sensor fusion for tractor autonomous guidance," in *Proc. IEEE Int. Conf. Autom. Logistics*, Aug. 2007, pp. 61–65.

[16] E. Nelson, "Developing an instrumentation package for in-water testing of marine hydrokinetic energy devices," in *Proc. OCEANS*, 2010, pp. 1–7.

[17] J. Echevarria, D. Blanco, J. Dominguez, J. Sanudo, and A. Alvarez, "Autonomous instrumentation system for offshore marine applications: Met-mast wind resource measurement implementation," in *Proc. IEEE Spain, OCEANS*, Jun. 2011, pp. 1–7.

[18] V. Kumar, S. Khalap, and P. Mehra, "Instrumentation for high-frequency meteorological observations from research vessel," in *Proc. OCEANS 2011*, pp. 1–10.

[19] R. Codeluppi, A. Golfarelli, A. Rossetti, P. Proli, A. Talamelli, and M. Tartagni, "A sensor network for real-time windsail aerodynamic control," in *Proc. ELMAR, 2010 PROCEEDINGS*, pp. 341–344.

[20] S. Corbetta, I. Boniolo, S. M. Savaresi, S. Vischi, A. Strassera, and D. Malgarise, "Real-time identification of the best performances of a sailboat," in *Proc. ACC*, 2011, pp. 4941–4946.

[21] H. Akimoto and H. Miyata, "Finite-volume simulation method to predict the performance of a sailing boat," *J. Marine Sci. Technol.*, vol. 7, no. 1, pp. 31–42, Jun. 2002.

[22] A. B. Philpott, S. G. Henderson, and D. Teirney, "A simulation model for predicting yacht match race outcomes," *Oper. Res.*, vol. 52, no. 1, pp. 1–16, Jan. 2004.

[23] Y. Masuyama, T. Fukasawa, and T. Kitazaki, "Investigations on sail force by full scale measurement and numerical calculation. (Part 1: Steady sailing performance)," *J. Soc. Naval Archit. Japan*, vol. 1997, no. 181, pp. 1–13, 1997.

[24] N. El-Sheimy, K. Chiang, and A. Noureldin, "The utilization of artificial neural networks for multisensor system integration in navigation and positioning instruments," *IEEE Trans. Instrum. Meas.*, vol. 55, no. 5, pp. 1606–1615, Oct. 2006.

[25] D. A. Grejner-Brzezinska, C. K. Toth, H. Sun, X. Wang, and C. Rizos, "A robust solution to high-accuracy geolocation: Quadruple integration of GPS, IMU, pseudolite, and terrestrial laser scanning," *IEEE Trans. Instrum. Meas.*, vol. 60, no. 11, pp. 3694–3708, Nov. 2011.

[26] S. Sabatelli, M. Galgani, L. Fanucci, and A. Rocchi, "A double-stage Kalman filter for orientation tracking with an integrated processor in 9-D IMU," *IEEE Trans. Instrum. Meas.*, vol. 62, no. 3, pp. 590–598, Mar. 2013.

[27] A. R. J. Ruiz, F. S. Granja, J. C. Prieto Honorato, and J. I. G. Rosas, "Accurate pedestrian indoor navigation by tightly coupling foot-mounted IMU and RFID measurements," *IEEE Trans. Instrum. Meas.*, vol. 61, no. 1, pp. 178–189, Jan. 2012.

[28] D. I. Katzourakis, E. Velenis, D. A. Abbink, R. Happee, and E. Holweg, "Race-car instrumentation for driving behavior studies," *IEEE Trans. Instrum. Meas.*, vol. 61, no. 2, pp. 462–474, Feb. 2012.

[29] P. M. G. Silson, "Coarse alignment of a ship's strapdown inertial attitude reference system using velocity loci," *IEEE Trans. Instrum. Meas.*, vol. 60, no. 6, pp. 1930–1941, Jun. 2011.
[30] J. Dias, M. Vinzce, P. Corke, and J. Lobo, "Editorial special issue: 2nd workshop on integration of vision and inertial sensors," *Int. J. Robot. Res.*, vol. 26, no. 6, pp. 515–517, Jun. 2007.
[31] P. Corke, J. Lobo, and J. Dias, "An introduction to inertial and visual sensing," *Int. J. Robot. Res.*, vol. 26, no. 6, pp. 519–535, Jun. 2007.
[32] E. Glancy and C. Harper, "Federal motor vehicle safety standards; occupant crash protection," Dept. Transp., Nat. Highway Traffic Safety Admin., Washington, DC, USA, Rep. NHTSA 99-6407, 1999.
[33] K. H. Kim, J. S. Ko, Y.-H. Cho, K. Lee, B. M. Kwak, and K. Park, "A skew-symmetric cantilever accelerometer for automotive airbag applications," *Sens. Actuators A, Phys.*, vol. 50, nos. 1–2, pp. 121–126, Aug. 1995.
[34] W. F. Milliken and D. L. Milliken, *Race Car Vehicle Dynamics*. Troy, MI, USA: Society of Automotive Engineers Inc., 1995.
[35] R. N. Jazar, *Vehicle Dynamics: Theory and Application*, 1st ed. New York, NY, USA: Springer-Verlag, 2008.
[36] *GPS Standard Positioning Service (SPS) Performance Standard*, U.S. Dept. Defence, Washington, DC, USA, 2008.
[37] *The Standard for Interfacing Marine Electronics*," NMEA Standard 0183, 2012.
[38] (2013, May 22). *Webbot Home* [Online]. Available: http://webbot.org.uk/iPoint/ipoint
[39] W. Sun, D. Wang, L. Xu, and L. Xu, "MEMS-based rotary strapdown inertial navigation system," *Measurement*, vol. 46, no. 8, pp. 2585–2596, Oct. 2013.
[40] R. S. Popovic, J. A. Flanagan, and P. A. Besse, "The future of magnetic sensors," *Sens. Actuators A, Phys.*, vol. 56, nos. 1–2, pp. 39–55, Aug. 1996.
[41] Y. Chen, N. E. Mendoza, Z. Nakao, and T. Adachi, "Estimating wind speed in the lower atmosphere wind profiler based on a genetic algorithm," *IEEE Trans. Instrum. Meas.*, vol. 51, no. 4, pp. 593–597, Apr. 2002.
[42] G. Ma, C. Li, J. Jiang, J.-Y. Liang, Y. Luo, and Y. Cheng, "A passive optical fiber anemometer for wind speed measurement on high-voltage overhead transmission lines," *IEEE Trans. Instrum. Meas.*, vol. 61, no. 2, pp. 539–544, Feb. 2012.
[43] J. M. M. Villanueva, S. Y. C. Catunda, and R. Tanscheit, "Maximum-likelihood data fusion of phase-difference and threshold-detection techniques for wind-speed measurement," *IEEE Trans. Instrum. Meas.*, vol. 58, no. 7, pp. 2189–2195, Jul. 2009.
[44] (2013, Jun. 6). *Weather Meters—SparkFun Electronics* [Online]. Available: https://www.sparkfun.com/products/8942
[45] *Weather Sensor Assembly p/n 80422 Data Sheet*, Argent Data Syst., Santa Maria, CA, USA, 2010.
[46] A. Bergeron, "Design and development of a marine data acquisition system for inertial measurement in wind powered yachts," M.A.Sc. thesis, Dept. Mech. Eng., University of Ottawa, Ottawa, ON, Canada, 2012.

Alexandre Bergeron received the Bachelor of Applied Science and Master of Applied Science degrees in mechanical engineering from the University of Ottawa, Ottawa, ON, Canada.

He is with the Royal Canadian Mint in Ottawa, ON.

Natalie Baddour received the B.Sc. degree in physics from the Memorial University of Newfoundland, St John's, NL, Canada, the M.Math degree from the University of Waterloo, Waterloo, ON, Canada, and the Ph.D. degree in mechanical engineering from the University of Toronto, Toronto, ON.

She held a Post-Doctoral position with the University of Toronto and the University of Bath, Bath, U.K. She is with the Department of Mechanical Engineering, University of Ottawa, ON, Canada, where she is currently an Associate Professor. Her current research interests include mathematical methods and algorithms, with applications to dynamics, vibrations, and biomedical engineering.